An examination of coherent noise in GOES-9 visible imagery

Dennis Chesters and Marit Jentoft-Nielsen
GOES Project
NASA Goddard Space Flight Center
Greenbelt, MD 20771
(Last updated 29 January 2002)

ABSTRACT

Coherent noise is analyzed for GOES-9 imagery observed on 8 January 2002. Anomalous semi-harmonic high-frequency noise is apparent in the visible imagery. Of the eight visible detectors, two detectors are found to have 10 counts RMS noise, four detectors have 5 counts RMS, and two detectors have 3 counts RMS (the normal value in GOES-8). The semi-harmonic noise observed in bright sunlit clouds is approximately twice the amplitude observed in dark space. The principal mode found by Fourier power spectra is a slowly modulated hum with a 4-to-6 visible sample period. Many other weak resonances are observed at longer periods. There are significant correlations in the anomalous noise among the visible detectors, with slow drifts in their mutual coherence over 30 minutes. No high-frequency anomalous noise is observed in the GOES-9 infrared channels, but there is anomalous behavior in the mean dark values near the assumed western space-clamps; west-to-east scans have significant line-to-line variations in channels 2 and 4, with different offsets for each detector.

INTRODUCTION

GOES-9 operated for 2.5 years as GOES-WEST before being turned off in 1998 when the momentum wheels became noisy. GOES-9 visible imagery was noticeably affected by a noticeable buzz along the scan lines that is believed to arise from vibrations in the bearings of the momentum wheels that provide 3-axis stabilization for the spacecraft. In December-January 2002, GOES-9 was brought out of cold on-orbit storage and operated for a few weeks in a near normal mode, delivering imagery that could be used for analysis.

This report analyses some GOES-9 imagery from 8 January 2002 for noise anomalies, mainly using Fourier power spectra and correlation statistics. This report discusses: 1) the problematic history of GOES-9, 2) the GOES-9 images being analyzed, and the underlying scan patterns, 3) the perceived semi-harmonic herringbone noise in the imagery, 4) the waveform and amplitude of the semi-harmonic noise on and off the Earth, 5) the power spectra, 6) the detector-to-detector correlations, 7) the statistics of the infrared channels, and 8) the results compared to GOES-8. Hyperlinks are provided to the web version of this report, and to a larger collection of intermediate results.

HISTORY

GOES-9 was launched in May 1995. After 7 months of on-orbit testing, it was put into operation as GOES-WEST at 135W in January 1996. It was commissioned with approximately 8.5 years of station-keeping fuel on board.

Soon after launch, a redundant winding in the Imager's scan mirror's motor failed. There was no loss of imaging performance, only of torque margin. NOAA and NASA devised a "mitigation" mode, turning off the instruments and tilting the satellite away from the Sun for 6 hours every night during spring and fall in order to minimize the highest temperatures on the winding, hopefully increasing the scan motor s lifetime.

In June 1998, momentum wheel #2 became obviously noisy and drew power spikes, as though the bearing was failing. NOAA shut off wheel #2 and started using a small spare wheel for attitude control, with momentum wheel #1 run faster to increase stiffness.

In early July 1998, momentum wheel #1 also started to demand more power and became fairly warm in order to maintain its rotation rate, as though its bearing was threatening to fail, too.

In mid-July 1998, GOES-9 was commanded back to normal 2-wheel mode. Wheel #2 continued noisy and drew near maximum power to maintain speed.

In August 1998, GOES-9 was shut down and put into cold storage on-orbit between 105 and 115 W (TBR).

In November 1999, GOES-9 was briefly spun up by NESDIS to perform orbit-maintenance maneuvers. NESDIS found the visible channel to still be noisy. It is not clear if any quantitative assessment of the noise was made at that time.

In December-January 2001-2, NESDIS again brought GOES-9 out of cold on-orbit storage and operated it in a near-normal scanning mode to gather data for analysis and to determine if the 3-axis system was rapidly failing.

On 17 January 2002, GOES-9 was returned to cold storage, with no new significant issues (TBR).

TEST IMAGES

During 7-11 January 2002, GOES-9 GVAR broadcast data was collected by the NASA ingest system at GSFC. The full disk image collected at 1420 UTC on 8 January 2002 is used for most of the following analysis. Other images were examined, and found to have similar noise characteristics. The 1420 UTC visible image is illustrated below in Fig 1-1.

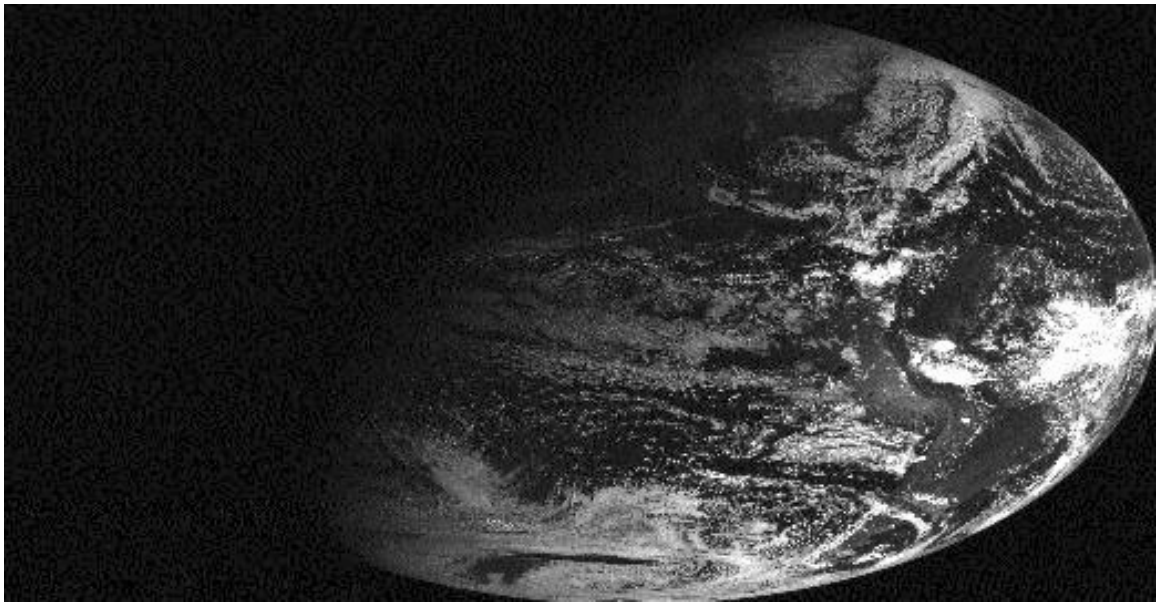

Fig. 1-1: Low-resolution picture from the GOES-9 full disk image at 1420 UTC on 8 January 2002.

The 1420 GMT image was selected because it was a half-illuminated Earth (sunrise over CONUS), providing a large number of dark pixels on the west limb for analysis of the noise in the baseline level of the visible channel. The west limb is also significant because it is close to the space clamp used every 2.2 seconds by the visible and infrared channels between every back-and-forth E-W scan of the Earth. Consequently, radiometric values could alternate their incoming and outgoing (even and odd scan line) characteristics.

During one GVAR broadcast scan, the data stream delivers 8 visible scan lines (1 km N-S resolution at nadir), 2 infrared scan lines in bands 2, 4 and 5 (2 km resolution), and 1 infrared scan line in channel 3 (8 km resolution). All detectors are over sampled along the E-W scan by a factor of 7:4, resulting in an picture that appears elongated in the E-W direction when samples are presented as square pixels, as in Fig 1-1. The visible sampling clock on GOES operates at 21,840 Hz, and the infrared clock at one-quarter that speed, 5,460 Hz. The full disk dataset represented by Fig. 1-1 required almost 30 minutes to acquire N-S.

NOISE CHARACTERISTICS

The full disk visible data set represented by Fig. 1-1 was formatted as 20836 samples along 10828 lines, with a TIFF header. Each pixel is a raw 10-bit count in an unsigned 16-bit integer value. In dark space, GOES visible baseline values are normally 29 counts, with 3 counts of RMS noise. The visible noise normally shows little coherence, other than very faint striping (difference in mean detector level). However, with GOES-9, the dark space to the left (western limb) of the 1420 UTC image presents a ragged herringbone pattern of semi-coherent noise, illustrated below in Fig. 2-1 and zoomed up in Fig. 2-2.

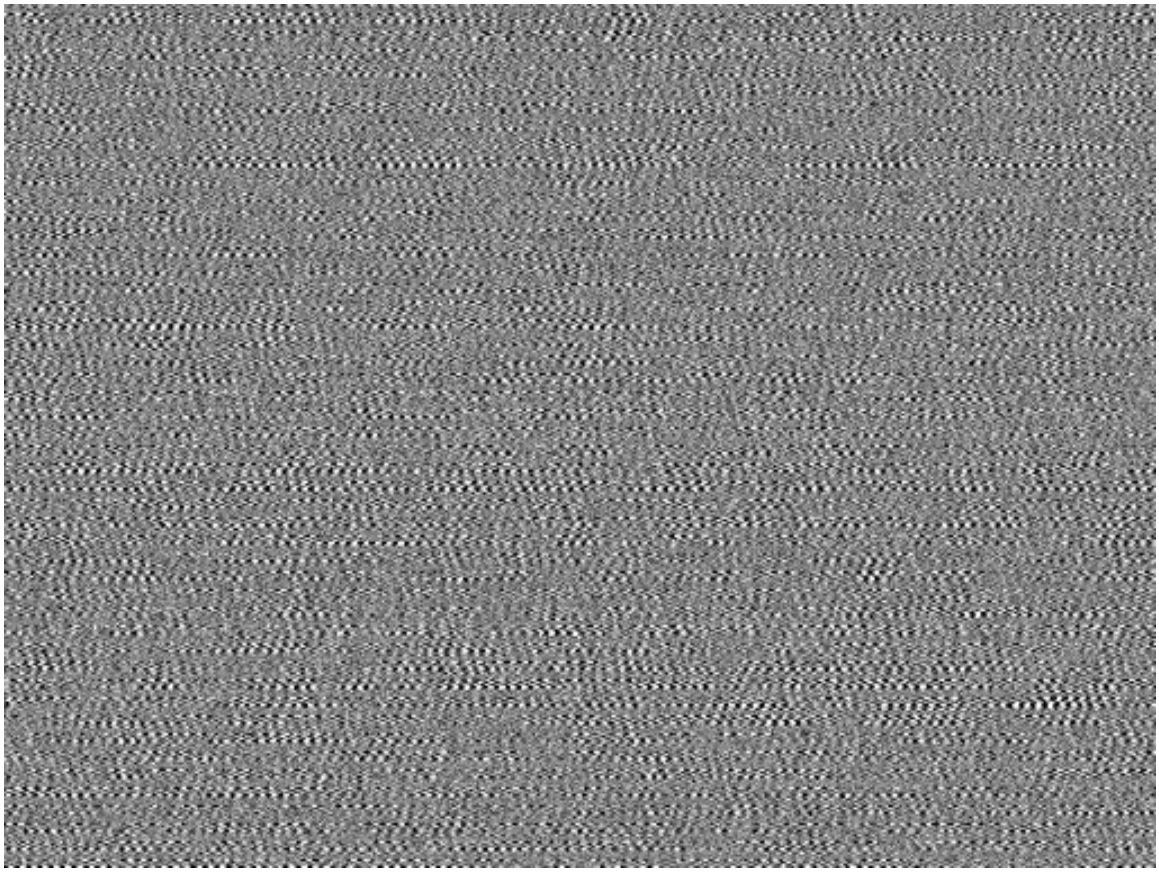

Fig 2-1: A contrast-enhanced 512x384 pixel section from the west edge of Fig. 1-1.

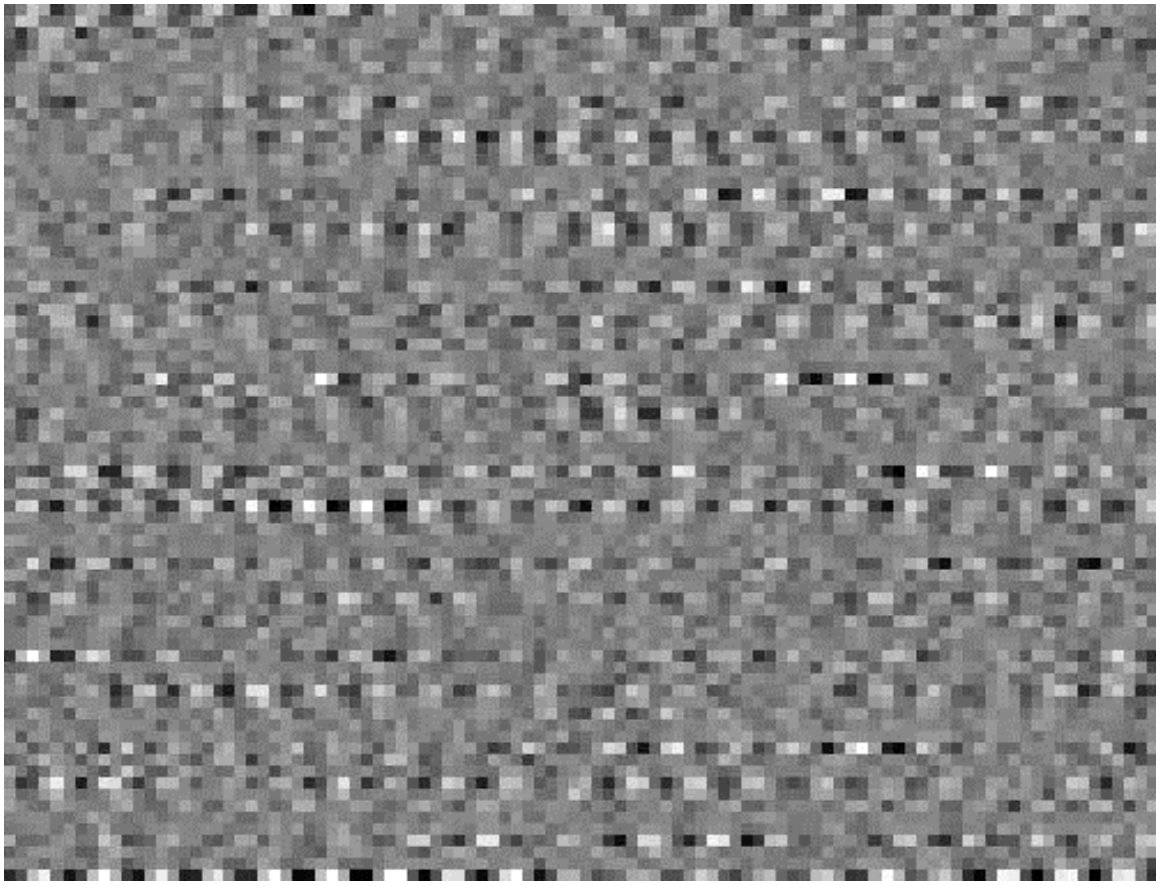

Fig. 2-2: A 5-fold zoom of the semi-coherent dark field noise in Fig 2-1.

The semi-coherent noise in Figs. 2-1 and 2-2 is stronger in some of the 8 visible detector lines. To obtain objective statistics, the dark field value histograms of the western 4096 samples for all 10,828 visible lines were calculated, grouped by logical detector (numbered 0 to 7 from north-to-south in groups of 8 per GVAR broadcast scan). Dark field count histograms for 3 groups of similar GOES-9 visible detectors are presented below in Figs. 2-3, 2-4 and 2-5.

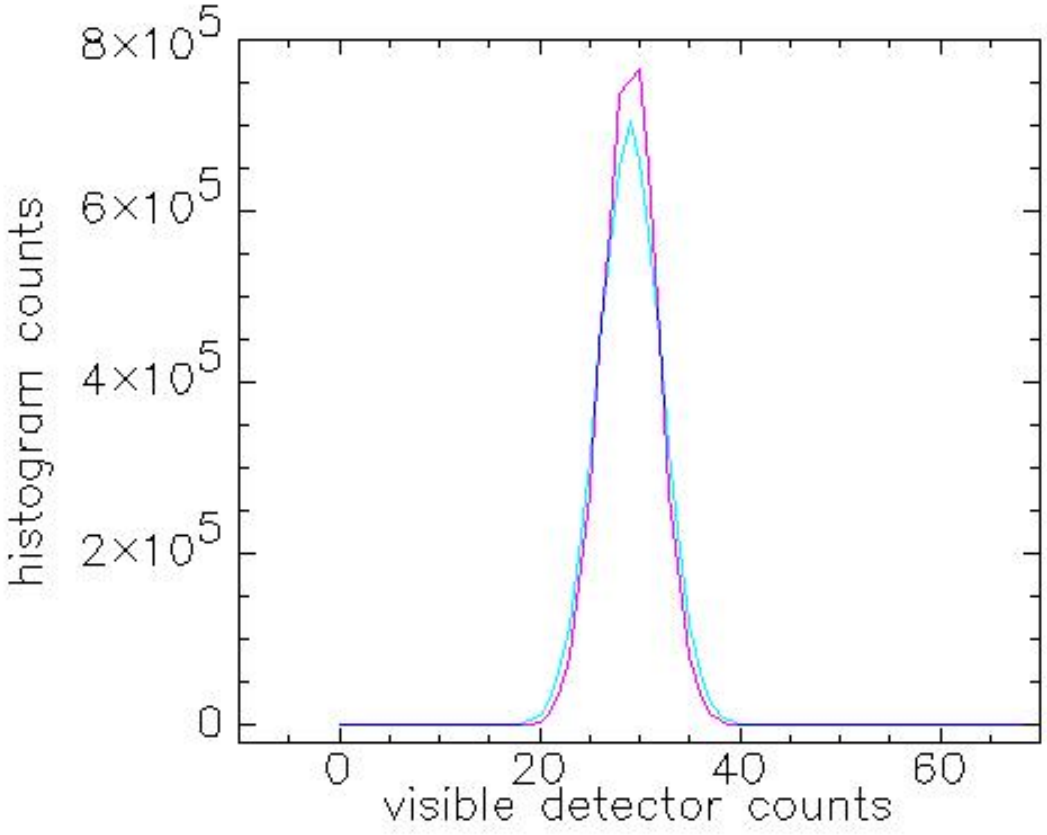

Fig. 2-3: Normal histogram of dark space visible count values from logical detectors 1 and 2.

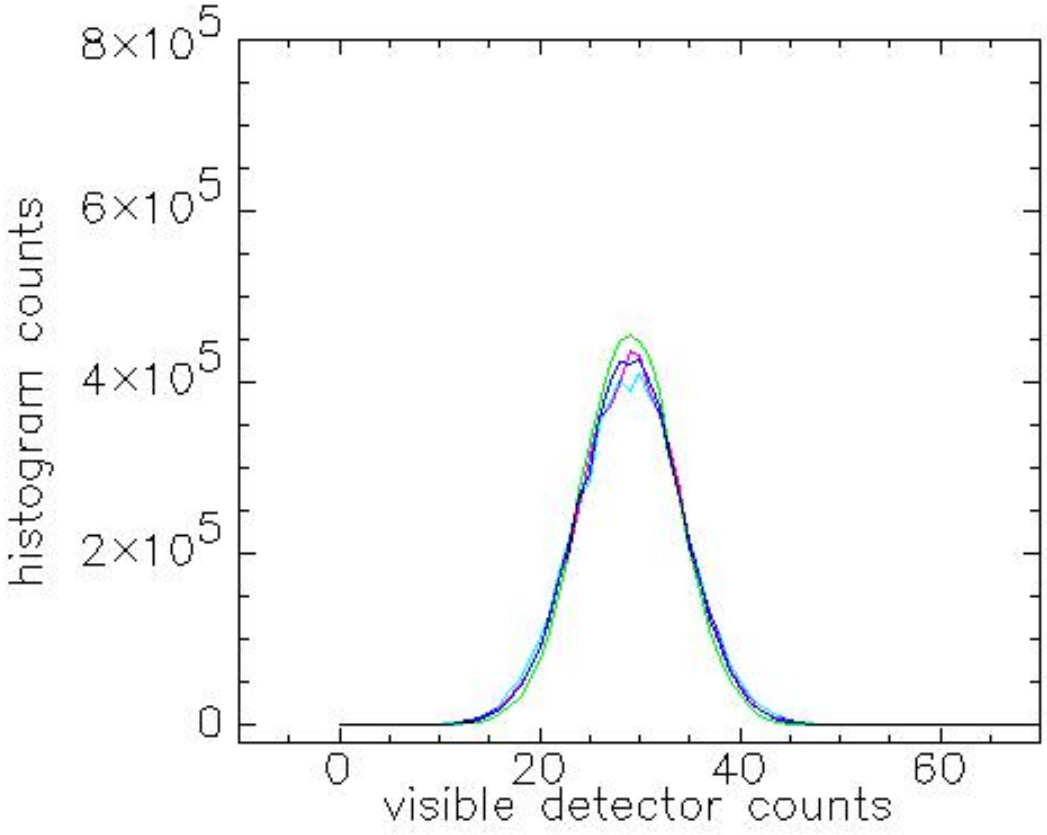

Fig. 2-4: Moderately noisy histogram of dark space visible count values for logical detectors 3, 4, 6 and 7.

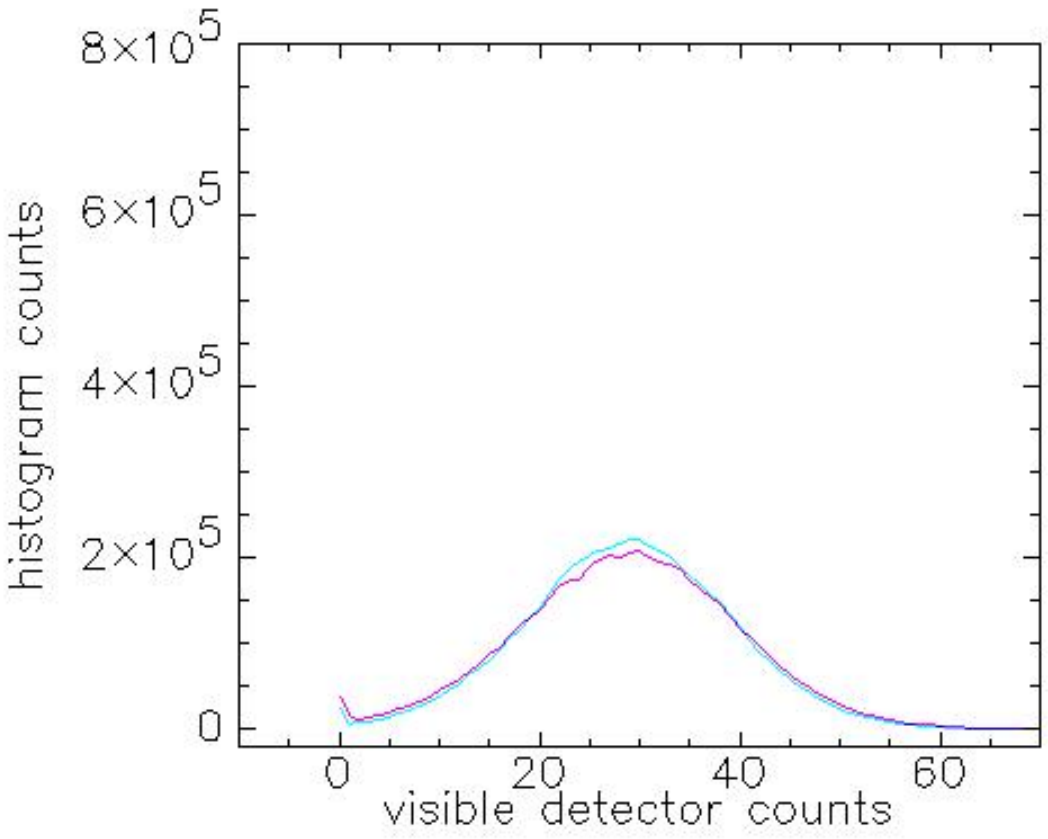

Fig. 2-5: Very noisy histogram of dark space visible count values for logical detectors 0 and 5.

Least-square fits of a Gaussian distribution to the GOES-9 dark field histograms in Figs 2-3/4/5 produce values for the width of the distribution from GOES-9 and for a similar (not shown) image from GOES-8. The Gaussian widths are presented in (Table 2-1), which also lists the correspondence between physical detectors 1-8 in the focal plane and logical detectors 0-7 in the broadcast GVAR data.

Table 2-1: Gaussian widths of the noise histograms for dark space values (digital counts) in Figs 2-3, 2-4 and 2-5 for GOES-9, compared to a similar analysis for GOES-8

Physical detector	Logical detector	GOES-9	GOES-8
5	**0**	10.0	2.8
6	**1**	3.2	2.9
7	**2**	2.8	2.6
8	**3**	5.4	2.7
1	**4**	5.2	2.7
2	**5**	10.7	2.8
3	**6**	4.8	2.9
4	**7**	5.1	2.7

NOISE ALONG A SCANLINE

The buzz in the visible imagery presented in Figs. 2-1 and 2-2 appears semi-harmonic when plotted as count values versus sample number along a scan line, such as in Fig. 3-1, below.

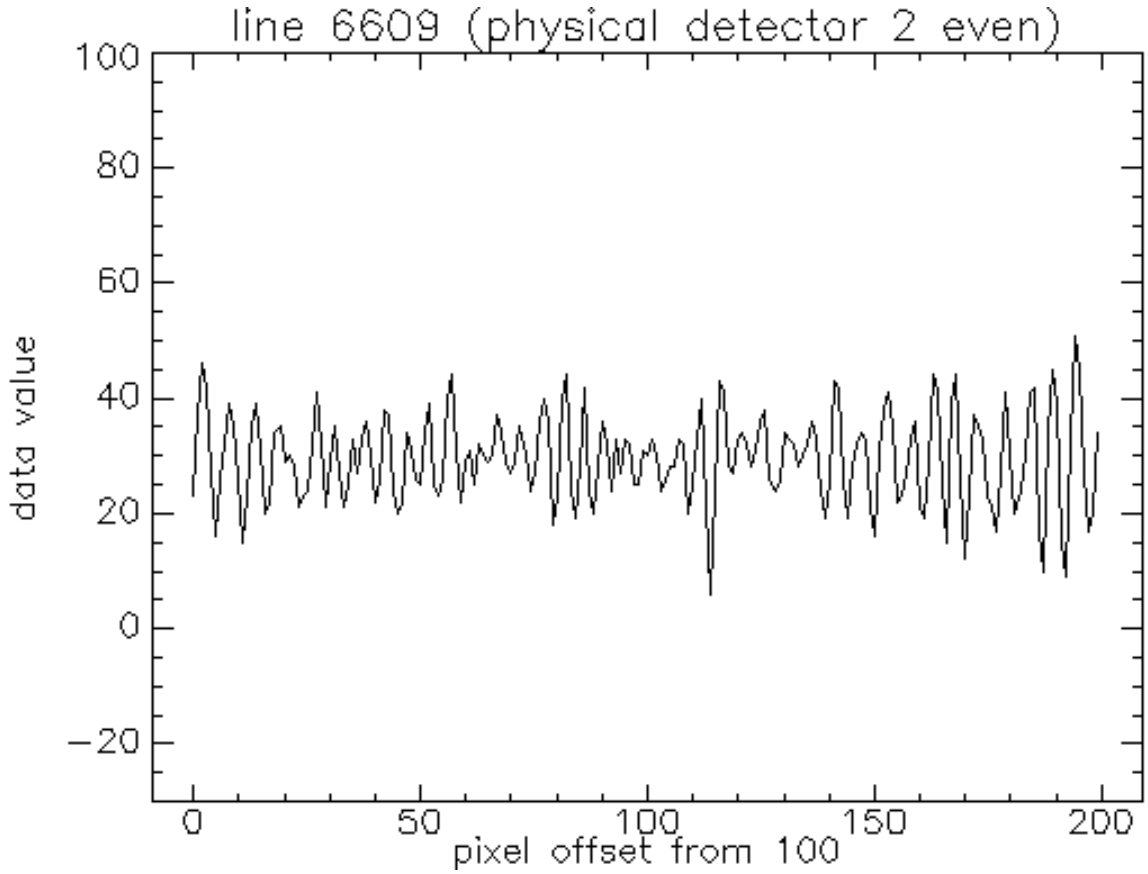

Fig. 3-1: Count values from visible detector 2 for 200 samples along scan line 6609, about half way down and near the left (western) edge of the GOES-9 full disk dataset illustrated in Fig. 1-1.

The fluctuations presented in Fig. 3-1 have a peak-to-peak range of approximately 20 counts centered on the nominal dark baseline value of 29 counts . The gain on GOES-9 visible imagery is such that 0-100% albedo is approximately 800 counts , so the apparent albedo of dark space observed by GOES-9 is 0%, fluctuating by 2.5%, peak-to-peak. The fluctuations have a dominant period of 4 to 6 samples, with a complex amplitude envelope over many 10 s of samples. Scan line fluctuations for all the visible detectors on GOES-9 are similar to Fig. 3-1, except for peak-to-peak amplitude.

An important issue for NOAA s use of the visible data is the effect of the semi-harmonic noise on sunlit clouds over the Earth. The scan line in Fig. 3-1 was selected near the N-S midpoint of the full disk scan, so that the same detector s scan line could be followed onto the bright cloud decks over the Equator, presented in Fig. 3-2.

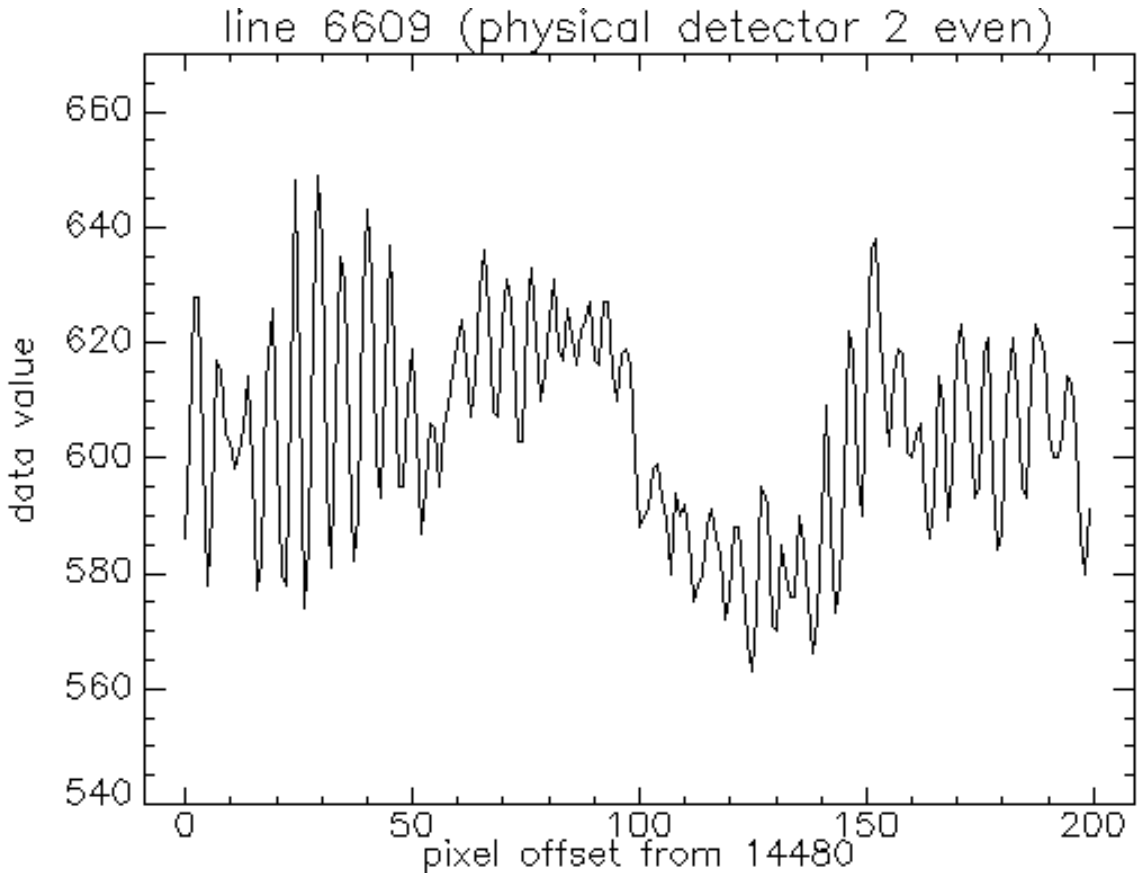

Fig. 3-2: Count values from visible detector 2 for 200 samples along scan line 6609, about half way down and near the middle (equatorial cloudy) section of the GOES-9 full disk dataset illustrated in Fig. 1-1.

The brightness fluctuations presented in Fig. 3-2 have a peak-to-peak range of approximately 40 counts around a bright cloud albedo of 600 counts . Here, the apparent albedo of bright clouds observed by GOES-9 is fluctuating by 5%, peak-to-peak. The fluctuations have a the same dominant period of 4 to 6 samples, with a complex amplitude envelope over many 10 s of samples, including cloud structure.

A comparison of Figs 3-1 and 3-2 indicates that the semi-harmonic noise is approximately double for a bright scene, compared to a dark scene. Consequently, the noise amplitude is non-linear in scene intensity. If the semi-harmonic noise is a multiplicative factor in the gain for the visible detectors, doubling implies that the dark current (subtracted off by the space clamp) is approximately equal to the additional current caused by the image of a bright cloud. Other interpretations are possible.

POWER SPECTRA

The semi-periodic behavior of the fluctuations presented in 2-1, 2-2 and 3-1, 3-2 suggest the use of Fourier analysis. The leftmost (dark field, western edge) 4096 samples of the image presented in Fig. 1-1 were converted to Fourier power spectra, line-by-line, for each of the 8 visible detectors.. Each spectrum is rather noisy. The ensemble of all the power spectra from logical detector 0 is presented below, in Fig. 4-1.

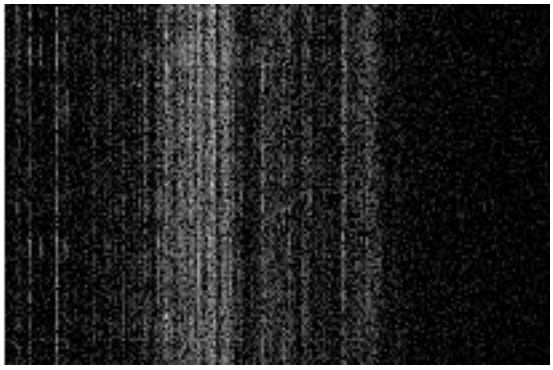

Fig. 4-1: Fourier power spectral density in line-by-line image format, from the westernmost dark field 4096 samples from all scan lines seen by logical detector 0.

The power for inverse sample frequencies from 0 (mean) to 2048 (sample-pairs) is plotted as intensity for each of the 1203 scan lines for detector 0 in Fig. 4-1. While there is some line-to line variation down through the image, there is a consistent suite of about 20 harmonics. This detector has the richest and strongest set of harmonics. The frequency and relative intensity of the many harmonics is similar from detector-to-detector (see the many fft illustrations at the hyperlink site).

Because the line-to-line power spectra are similar in Fig. 4-1, it is reasonable to add them together and present them as a composite power-frequency plot for the entire image. A sample spectrum is presented in Fig. 4-2 for logical detector 0.

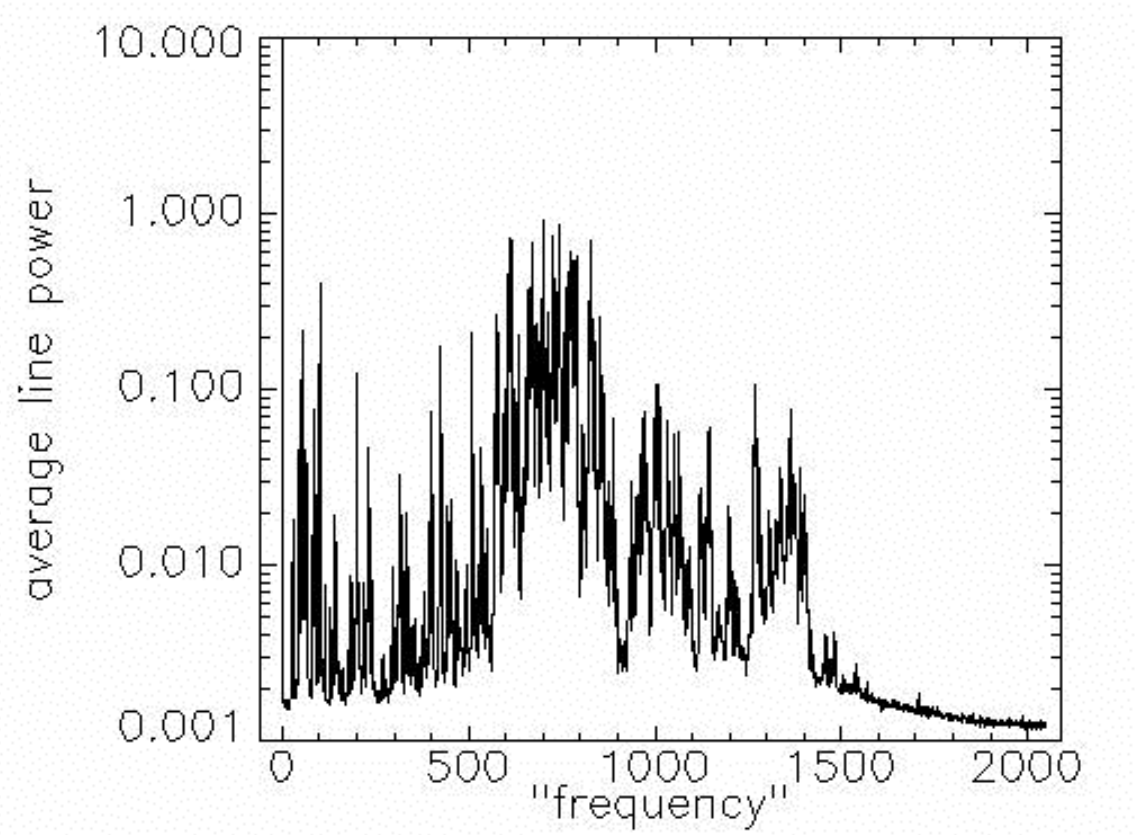

Fig 4-2: Composite power spectral density from the westernmost dark field 4096 samples from all scan lines seen by logical detector 0. Power is plotted on a logarithmic scale.

The strongest harmonic in Fig. 4-2 is a broad peak spanning the frequency band of 700 to 800 inverse samples, which corresponds to a 5-to-6 sample periodicity (4096/5 = 819 and 4096/6 = 683). Secondary peaks occur around frequencies of 1000 and 1350 inverse-samples, which correspond to sampling periods around 4 and 3 clock ticks, respectively, at 20,380 Hz.

The power as a function of sampling interval is better presented by plotting the spectra using 1/frequency from the abscissa of Fig 4-2. In the following Figs. 4-3, 4-4 and 4-5, the composite power spectra for detector 0 are plotted for sampling ranges 2-16, 8-64 and 32-256, respectively. Overlap in the sampling range is provided for continuity.

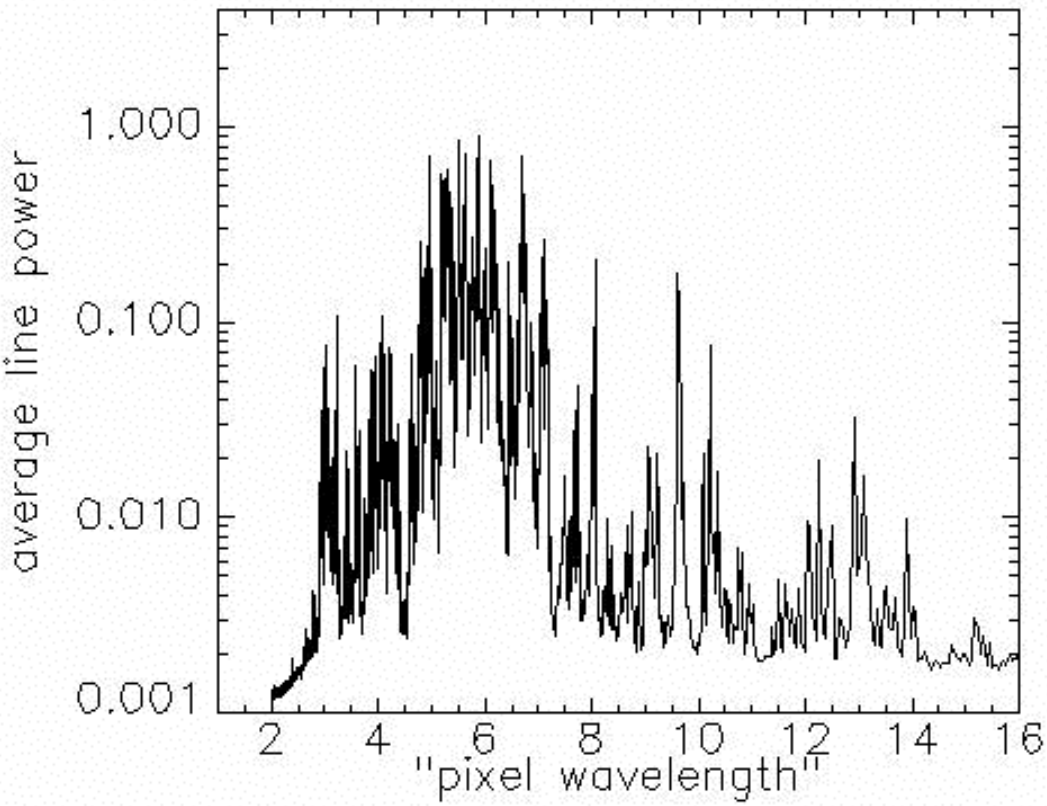

Fig 4-3: Composite power spectral density from the westernmost dark field 4096 samples from all scan lines seen by logical detector 0. Power is plotted on a logarithmic scale versus sampling interval for the sampling range 2-16.

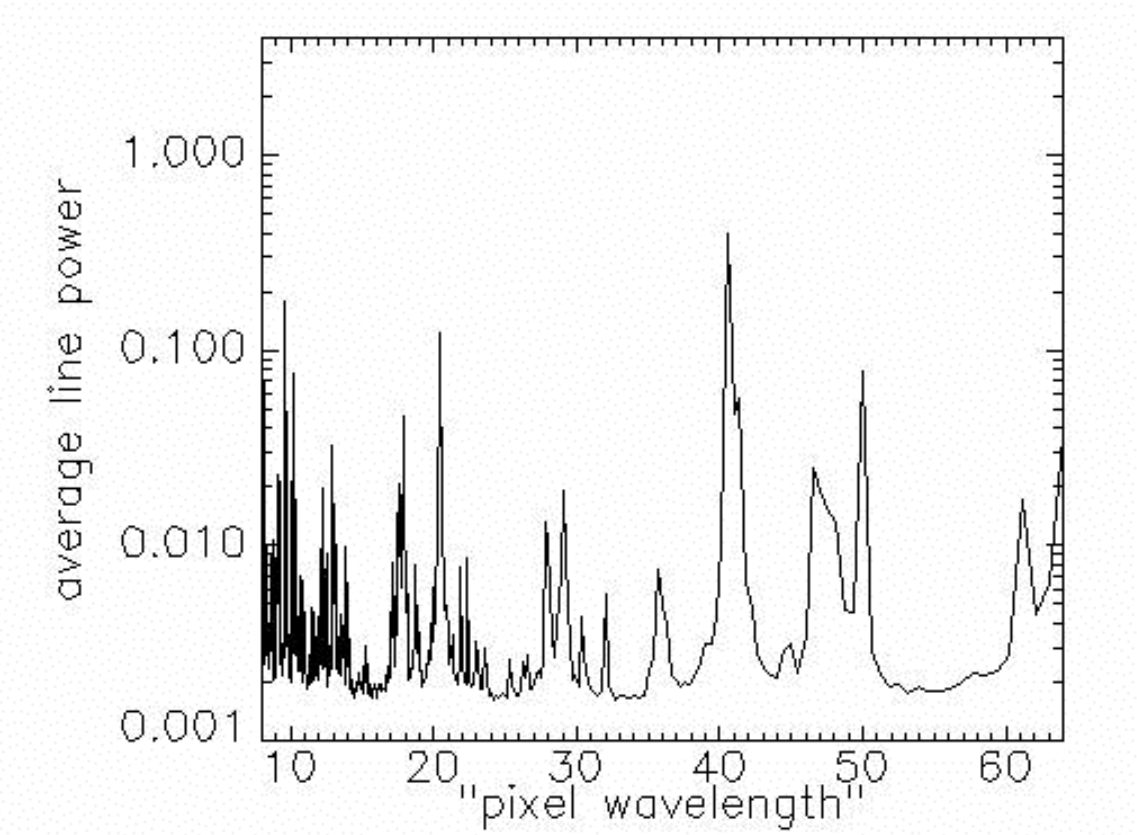

Fig 4-4: Composite power spectral density from the westernmost dark field 4096 samples from all scan lines seen by logical detector 0. Power is plotted on a logarithmic scale versus sampling interval for the sampling range 8-64.

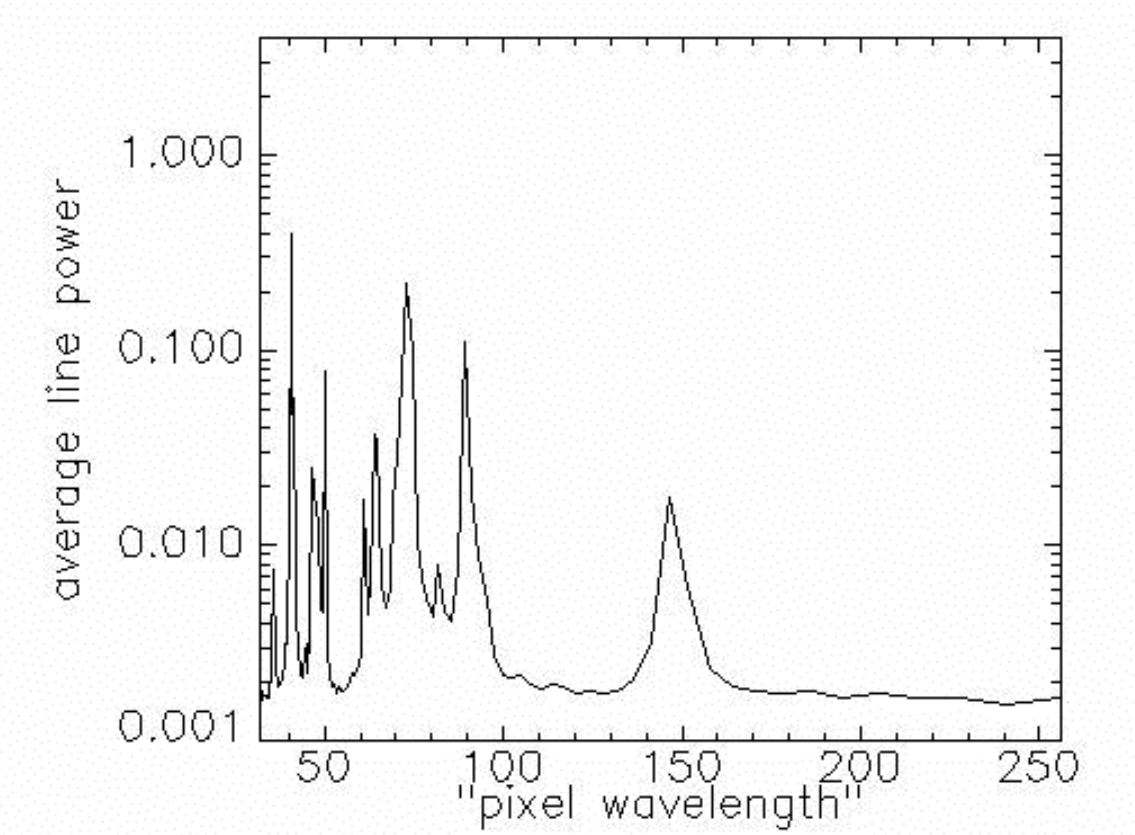

Fig 4-5: Composite power spectral density from the westernmost dark field 4096 samples from all scan lines seen by logical detector 0. Power is plotted on a logarithmic scale versus sampling interval for the sampling range 32-256.

In addition to the high-frequency resonances already recognized at 3, 4 and 5-to-6 sampling rates in Fig 4-2, Fig 4-3 indicates that detector 0 has resonances near 8.0, 9.2, 9.6, 10.5 and 13.0 samples. Likewise, Fig. 4-4 indicates resonances near 17.5, 21, 42, 48 and 50 samples. Finally, Fig. 4-5 indicates resonances near 75, 90, and 150 samples.

Because these power spectra are composites of millions of samples, they are capable of detecting unusual resonances at the level of 1/100 of a count, as further illustrated with detector 4 s spectrum in Fig. 4-6.

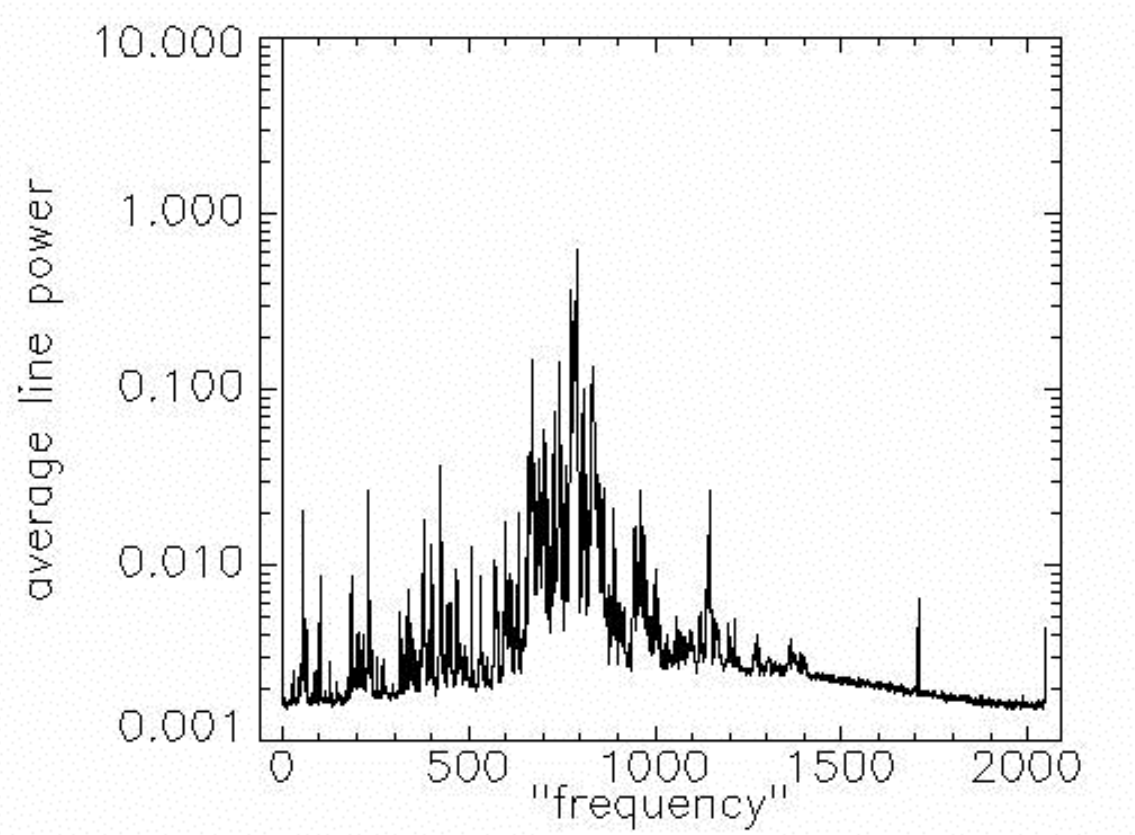

Fig. 4-6: Composite power spectral density from the westernmost dark field 4096 samples from all scan lines seen by logical detector 4. Power is plotted on a logarithmic scale.

Similar to detector 0 in Fig. 4-2, Fig. 4-6 shows a main power resonance for detector 4 at 700 to 800 inverse samples. In addition, there are weak but sharp resonances at 1140 and 1710 inverse samples, which correspond to approximately 3.6 and 2.4 sample rates, respectively, at 20,380 Hz.

These results indicate that the microphonic (acoustic-to-radiometric) sensitivity of the visible detectors on GOES could be use to monitor the mechanical health of the satellite by listening to low level vibrations to a fraction of a count and a fraction of a sampling interval. Tracking the power spectra in the visible dark scenes with time could be used characterize the aging of the mechanical systems on the GOES satellites.

DETECTOR-TO-DETECTOR CORRELATIONS

The GOES-9 visible detectors have somewhat similar power spectra, and the herringbone patterns found the noisy dark field images in Figs 2-1 and 2-2 indicates that there is some correlation among detector fluctuations.

However, one set of GVAR scan records does not contain visible samples that are contemporaneous. The top 4 visible lines from an scan approaching the western clamp were really collected during the previous outgoing physical scan, due to the 4 km N-S optical offset of the 8 visible detectors with respect to the infrared detectors. This is important when doing time-based correlation between detectors, since there can be a 2 second difference between the observation time of the top 4 and bottom 4 visible detectors. The physical detector numbers are embedded in the GVAR scan line headers, and these are used to properly account for detector-to-detector correlations. The list of physical-to-logical detector numbers was previously presented in Table 2-1.

The following analysis will use physical detector numbers to calculate correlations between detectors, in order to group together contemporaneous observations. In addition, the scan lines are separated according to the direction of scan by separation of even and odd scan numbers into separate groups. It is not yet clear if scans incoming/outgoing from the western space clamp are odd/even or even/odd.

To calculate detector-to-detector correlation, the variation in count along the 4096 west most dark field values from each physical detector had the mean value for the line subtracted, and the residual was normalized by the RMS value of the residuals for that detector-line. The normalized residuals were then correlated with the corresponding residuals for another detector in the same physical scan. This was done for each of even/odd physical scan lines (E-to-W and W-to-E), approximately 1280 correlations in all. Each correlation value is measured near the GOES Imager space clamp that occurs every 2.2 seconds on the limb furthest from the Sun.

Therefore, the 1280 detector-to-detector correlations represent the mean value for 4096 samples every 2.2 seconds for the duration of the image scan, approximately 30 minutes. Fig 5-1 presents one such correlation plot for physical detectors 1 and 5.

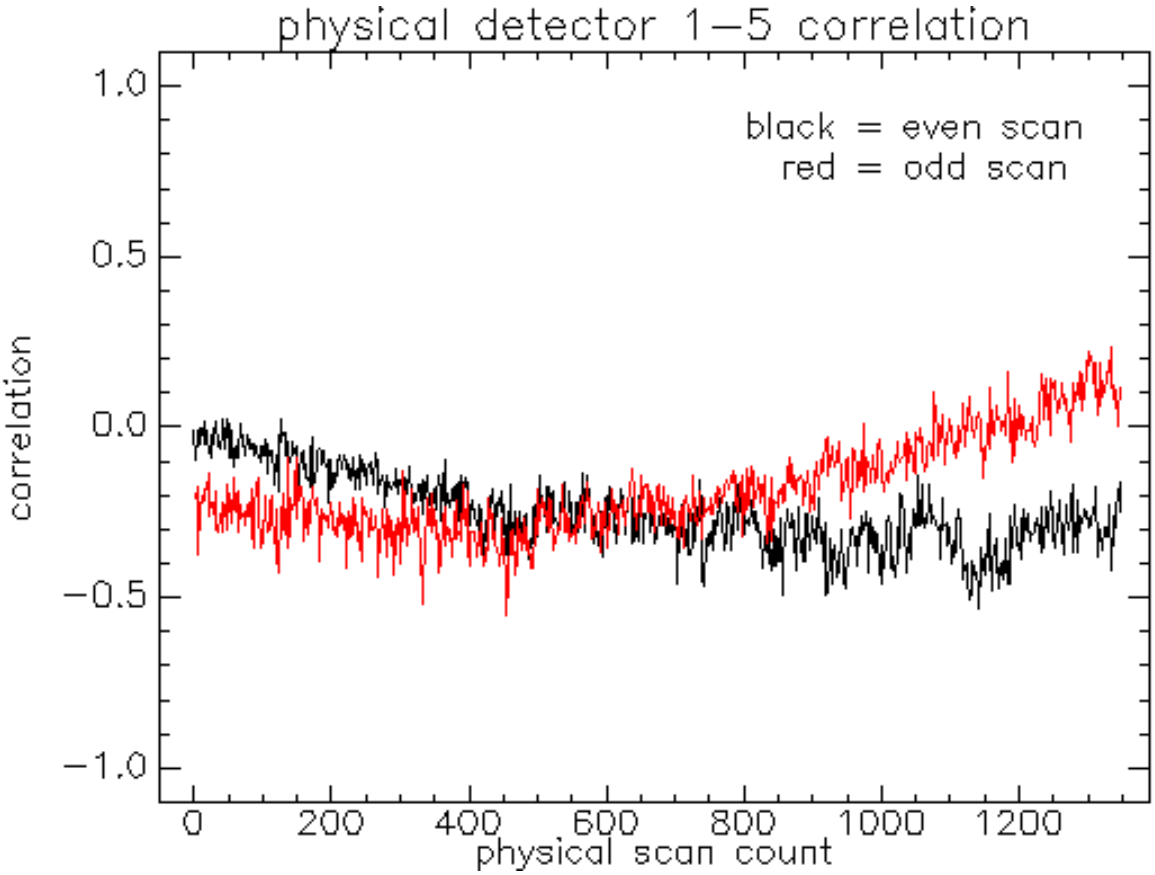

Fig. 5-1: Correlations between the physical detectors 1 and 5 for all the visible scan lines in the GOES-9 full disk image, with separate correlations for odd and even scans.

If the fluctuations in detector values were random with respect to each other, the correlations would be near zero. However, Fig. 5-1 indicates that the correlations between GOES-9 visible detectors are: 1) significantly non-zero, 2) significantly different for odd and even scans, and 3) significantly drifting in time while the full disk image is being scanned.

The GVAR line header indicates that values for an even scan count correspond to a line outgoing from the assumed western space clamp (just after the clamp, scanning from west-to-east).

There are 8 physical detectors to correlate in every combination, resulting in a zoo of correlation behavior, presented in Table 5-1. Each cell in the table contains a thumbnail image like the more detailed plot in Fig. 5-1. Auto-correlations and redundant permutations are left blank in Table 5-1. The detector 1 column was omitted from Table 5-1 to make the table fit on a page. A full presentation of Table 5-1 is available at the hyperlink list at the end of this report.

Table 5-1: Correlations between the 8 physical detectors for all the visible scan lines in the GOES-9 full disk image, with separate correlations for odd and even scans.

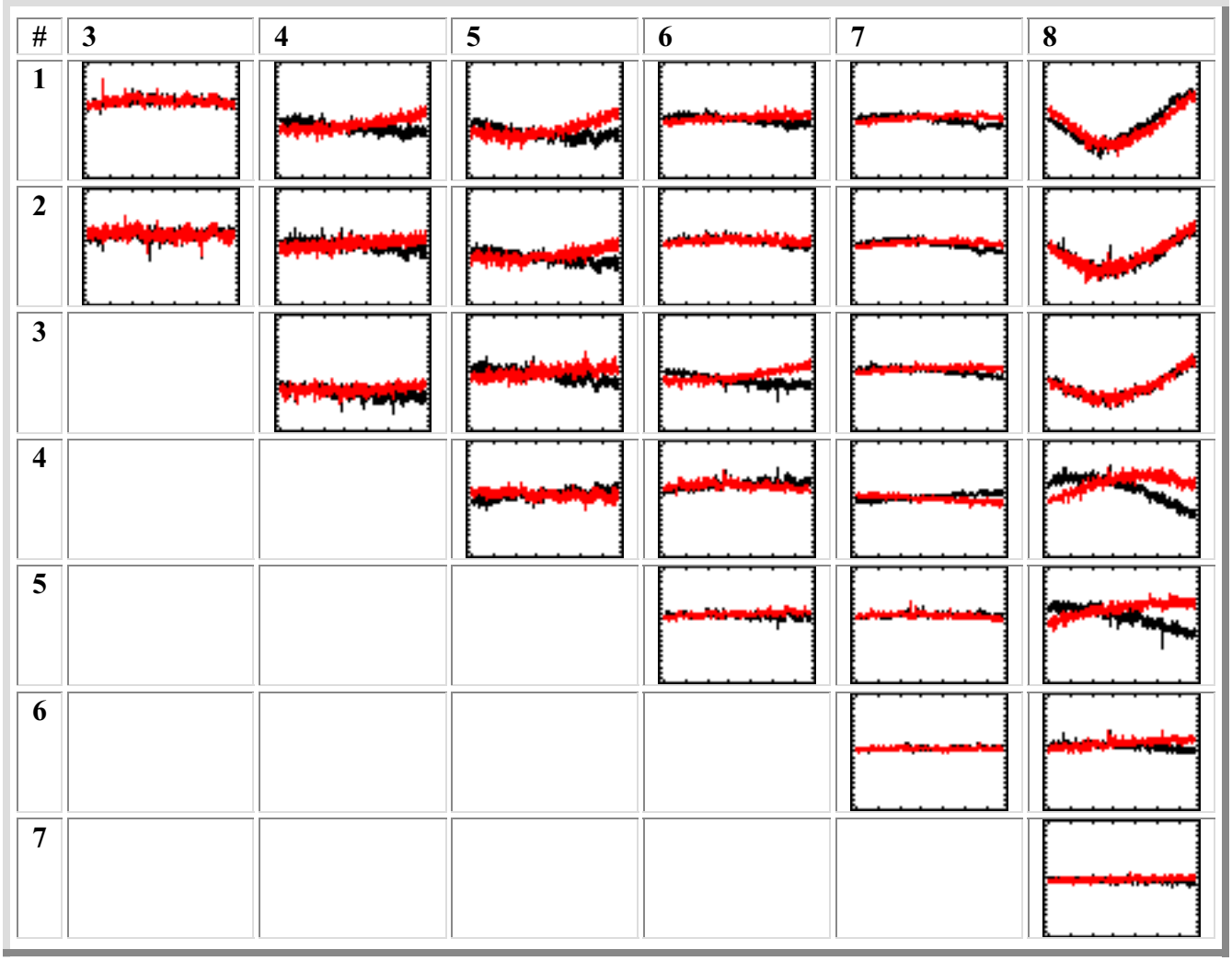

The time-drift correlations among GOES-9 visible detectors presented in Table 5-1 are often non-zero and without an obvious pattern. Physical detector 1 has significant positive correlation with detectors 2 and 3. Physical detector 8 has strong but slowly varying correlations with detectors 1, 2 and 3, scan-direction dependent correlations with detectors 4 and 5, and little correlation with detectors 6 and 7.

INFRARED DETECTORS

The corresponding GOES-9 infrared channels were examined for anomalous noise values in the west most view of outer space. Greyscale imagery showed no quasi-harmonic herringbone patterns like those observed in the visible channels. If there were fluctuations at the rate of a few visible clock samples, they would not be apparent in the infrared data, because it is sampled at one-quarter the rate. A low-resolution view of the Earth is presented in Fig. 6-1 from channel 2.

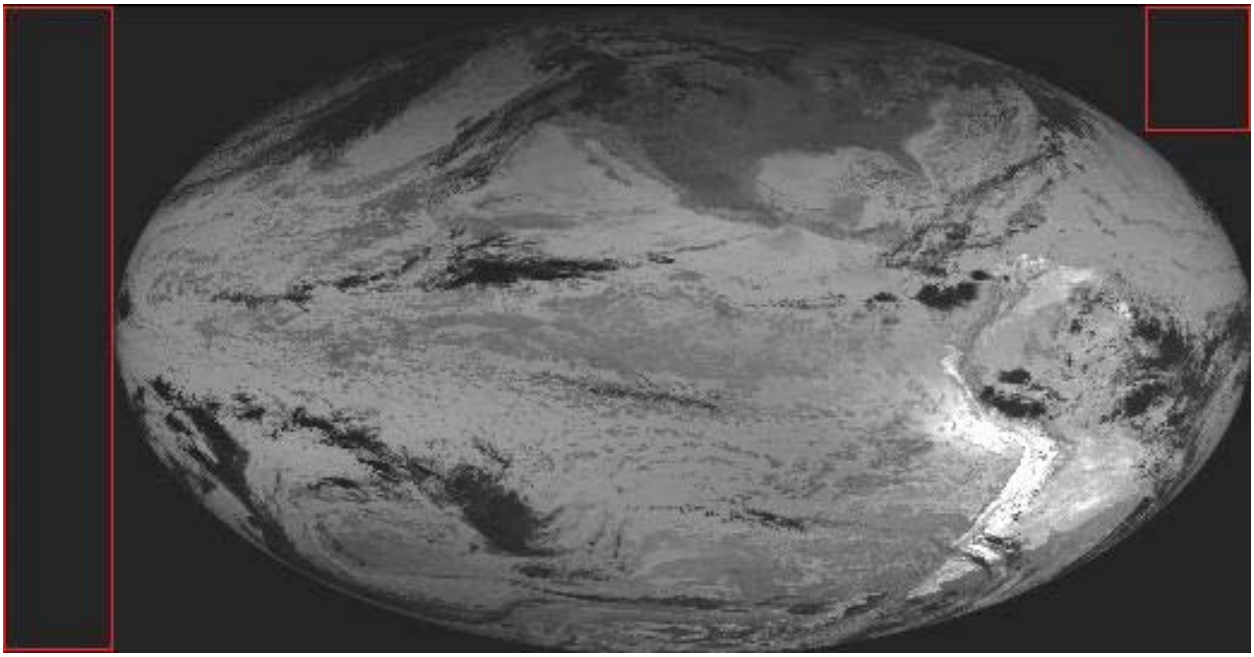

Fig. 6-1: GOES-9 image of the Earth at 1420 UTC on 8 January 2002 in channel 2 (4 microns).

A statistical and power spectrum analysis of the west most dark field values for the GOES-9 infrared bands revealed nothing significant. However, unusual histograms in the noise values lead to the detailed examination of the dark field values separated by detector and odd/even (incoming and outgoing) scan lines. Figs. 6-2 through 6-8 present the mean value of the western dark field scan line for each channel and detector, with the odd/even scan directions indicated with red/black dots.

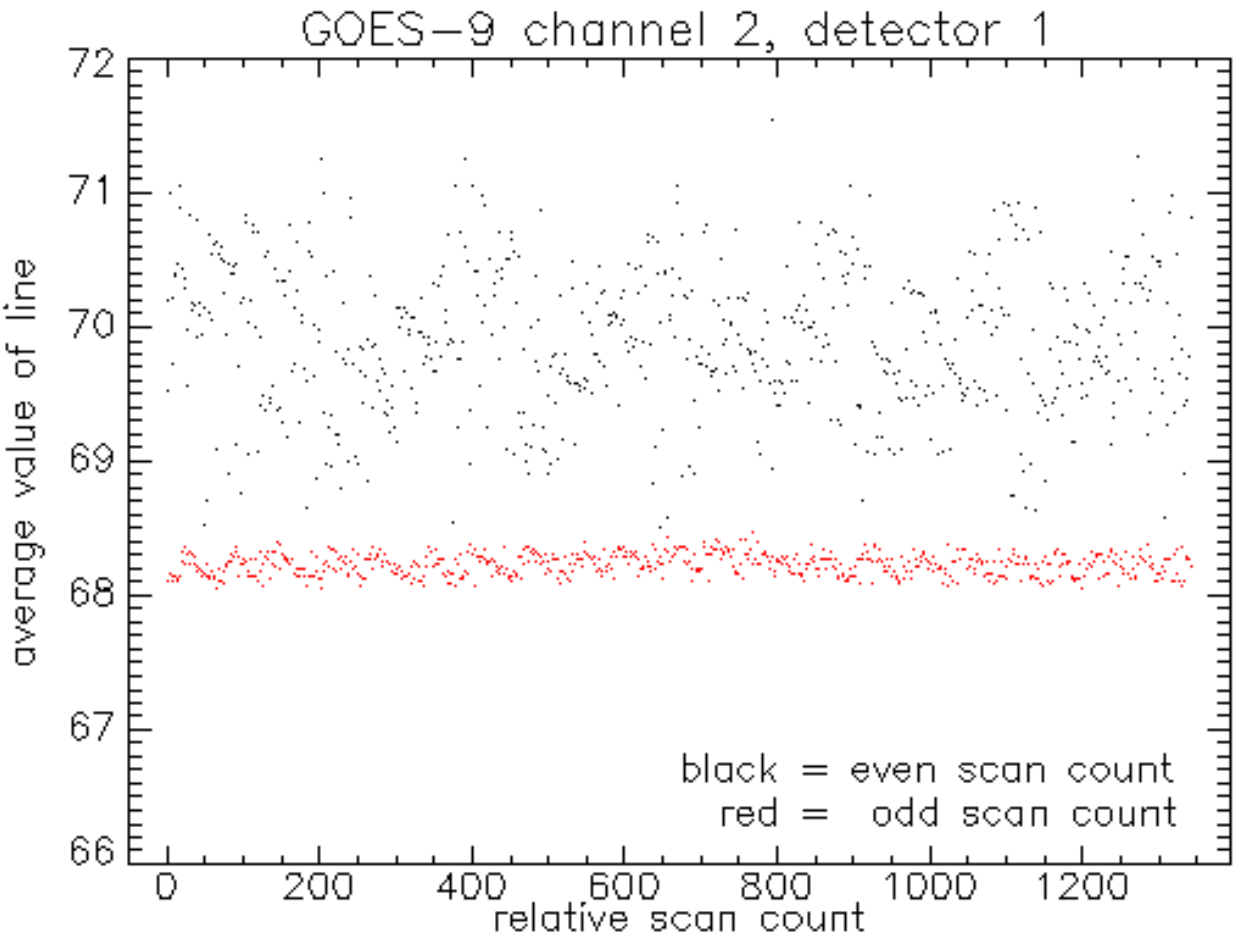

Fig. 6-2: Line-by-line mean dark field values in counts for channel 2, detector 1.

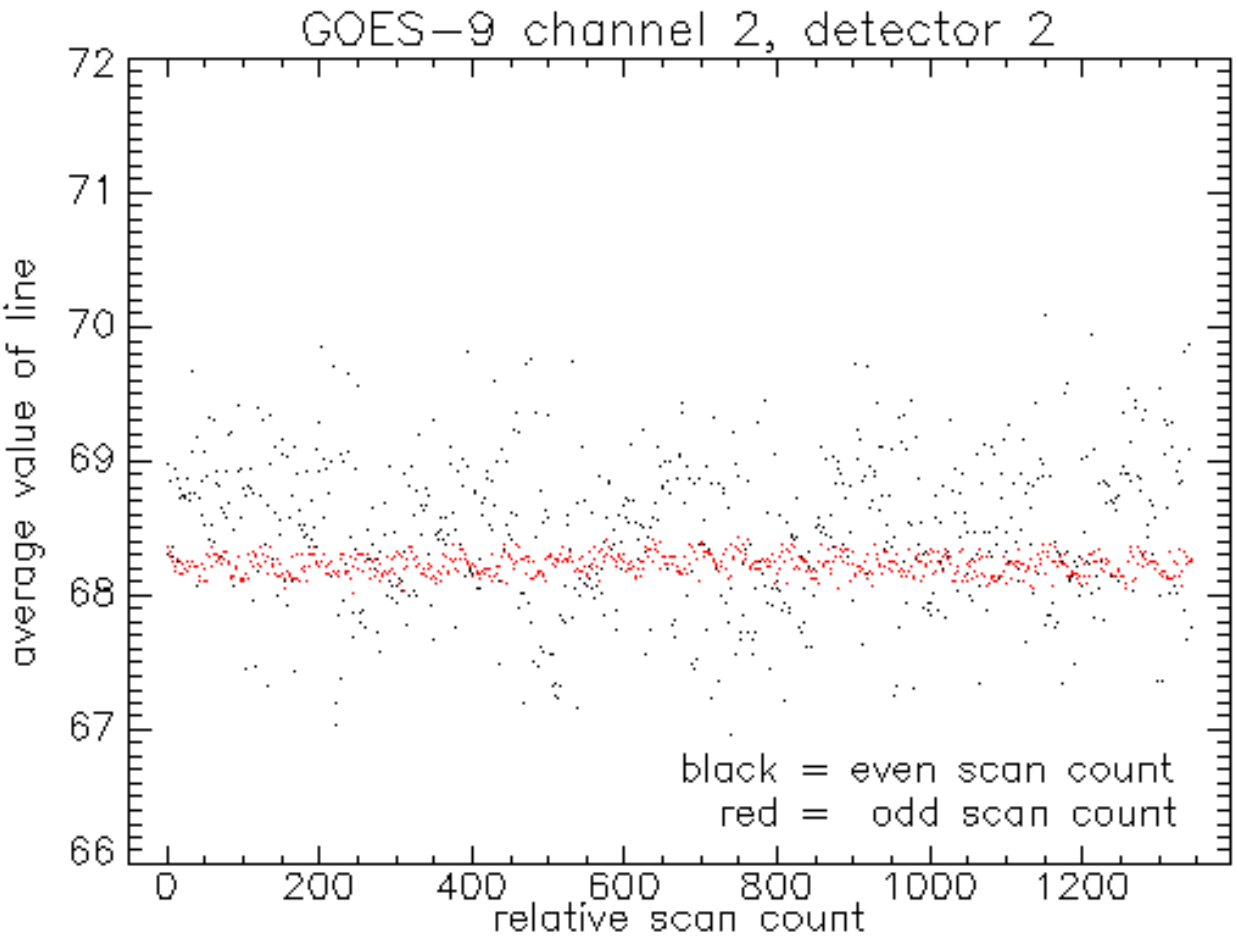

Fig. 6-3: Line-by-line mean dark field values in counts for channel 2, detector 2.

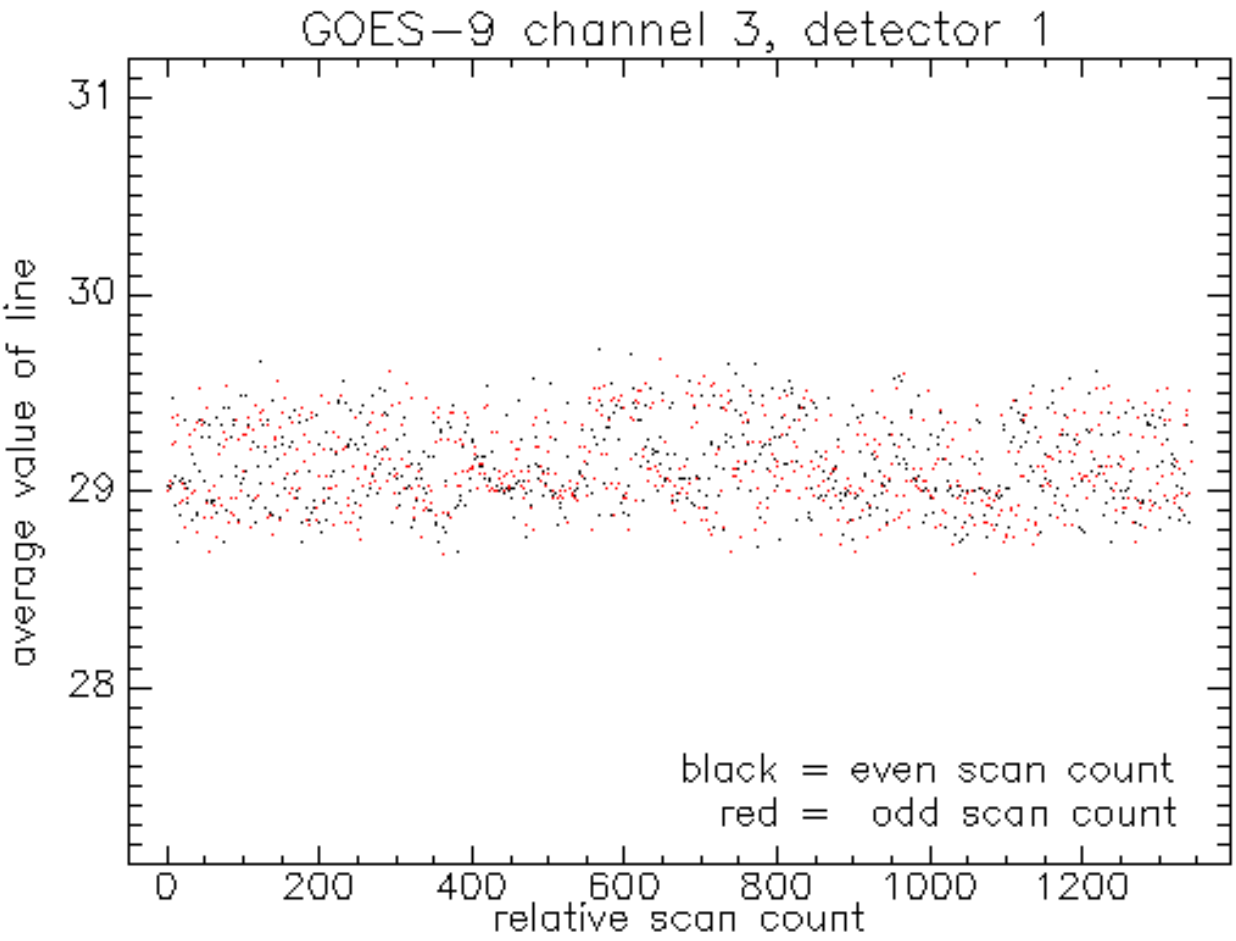

Fig. 6-4: Line-by-line mean dark field values in counts for channel 3, only 1 detector.

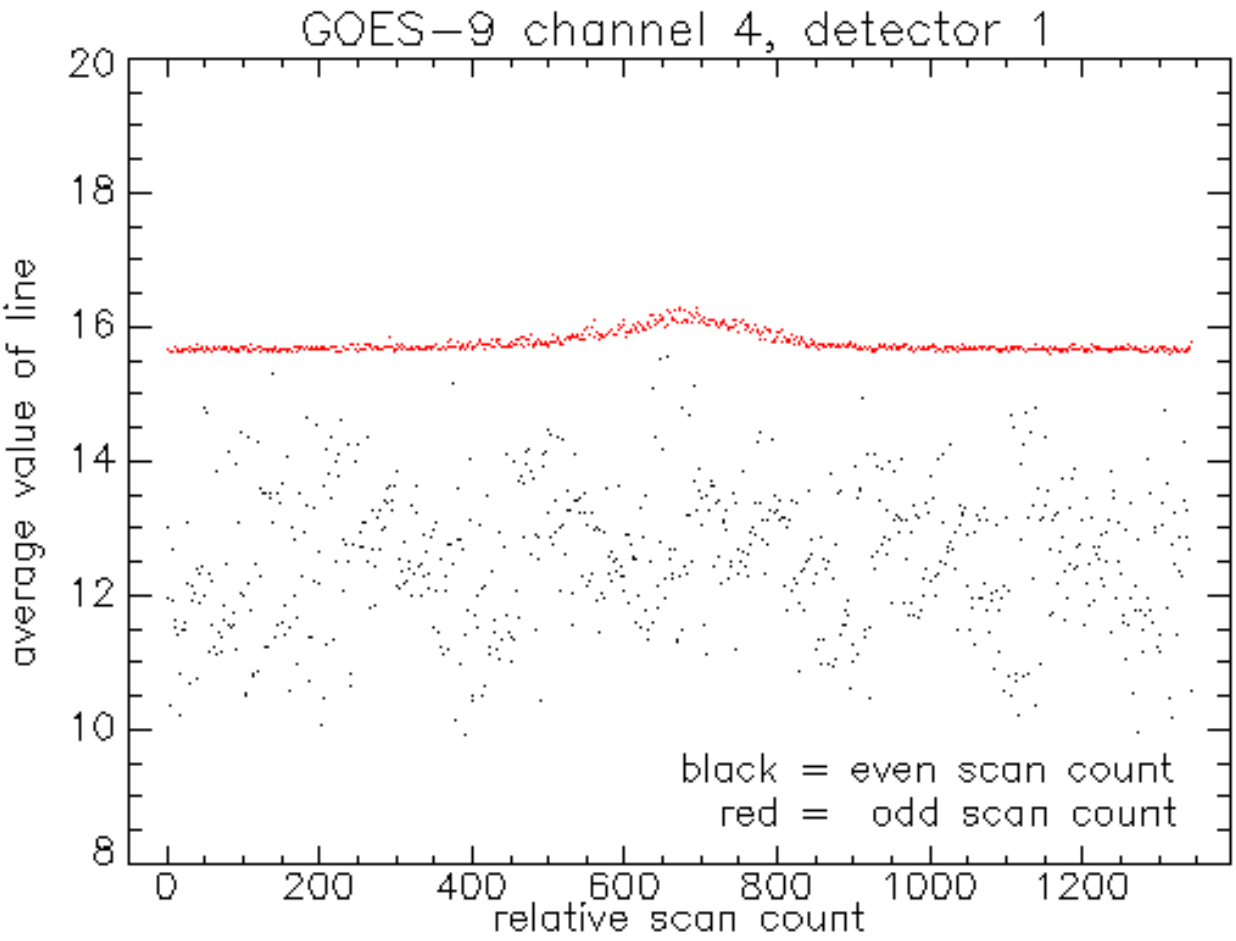

Fig. 6-5: Line-by-line mean dark field values in counts for channel 4, detector 1.

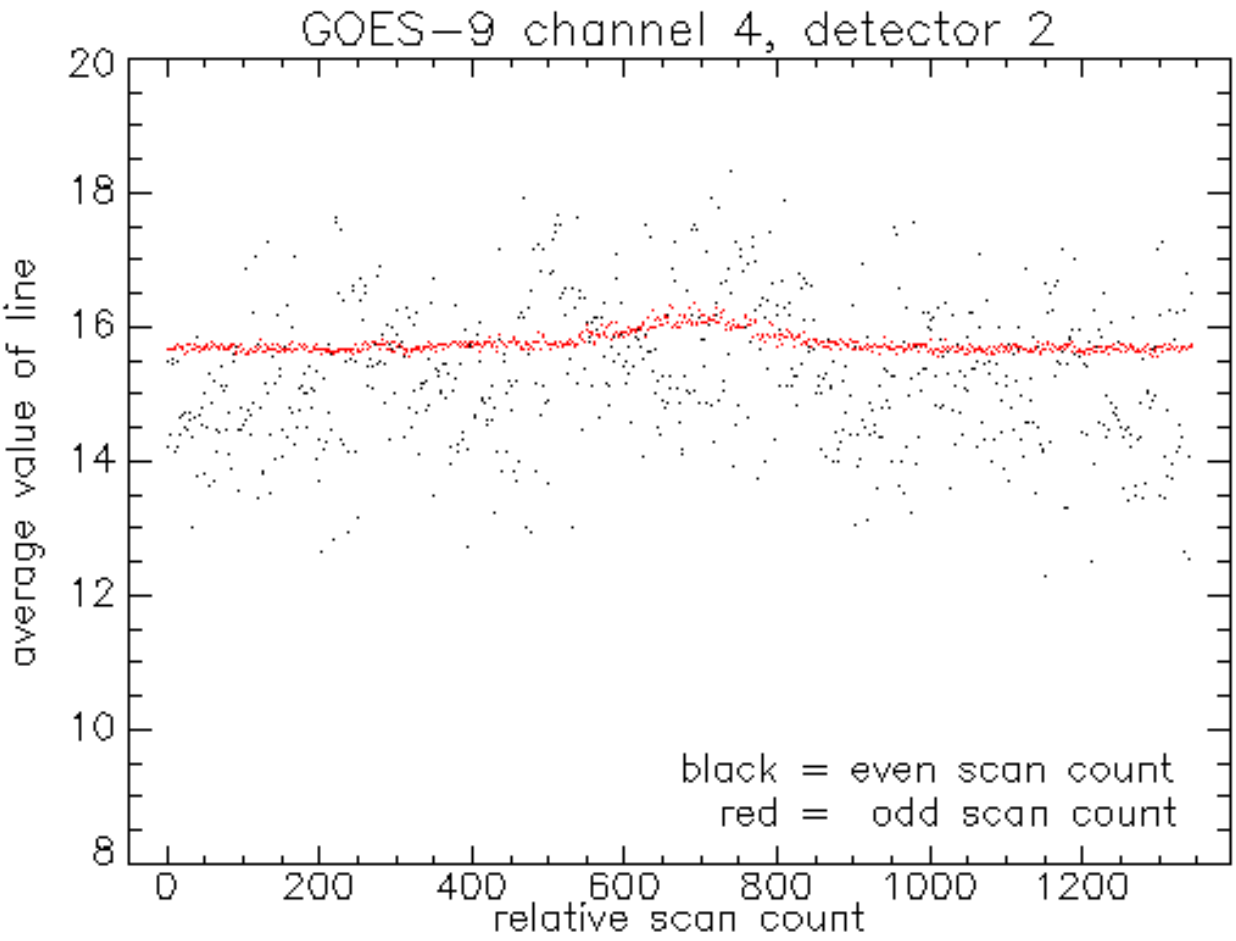

Fig. 6-6: Line-by-line mean dark field values in counts for channel 4, detector 2.

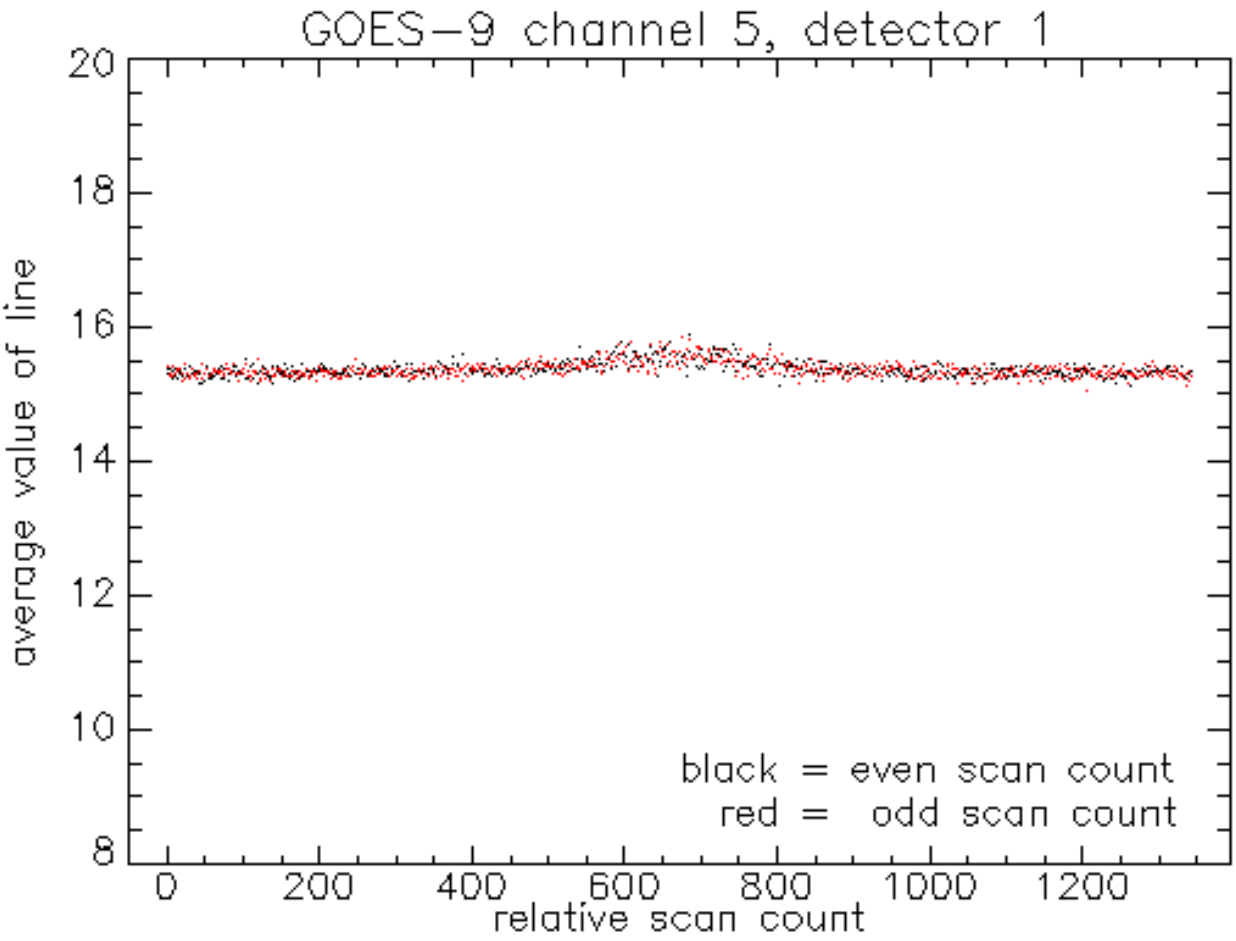

Fig. 6-7: Line-by-line mean dark field values in counts for channel 5, detector 1.

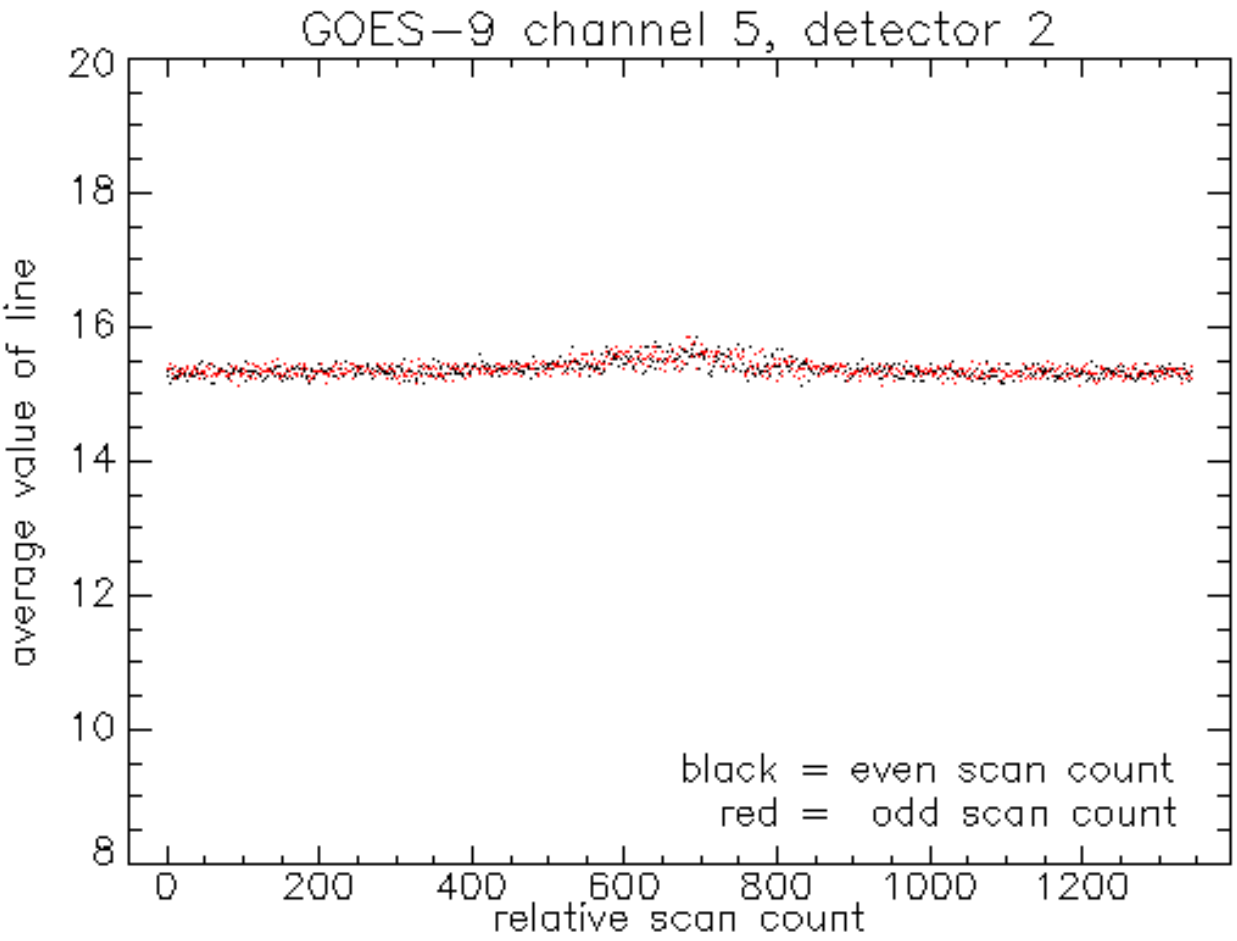

Fig. 6-8: Line-by-line mean dark field values in counts for channel 5, detector 2.

For both infrared detectors in channel 2 and channel 4, there is a significant offset and scatter about the mean dark space values that depends upon the odd/even (incoming/outgoing) status of the scan line. The GVAR line header indicates that values for an even scan count correspond to a line outgoing from the assumed western space clamp (just after the clamp, scanning from west-to-east). Curiously, channels 3 and 5 are not likewise affected. The slight rise in the dark field mean near the center of the plots is due to the selection box grazing the western infrared limb of the Earth, as shown in Fig. 6-1.

The infrared dark field anomalies seem more likely due to errors in ground-based calibration software and/or the values of the space clamp data than in vibration-induced detector errors.

COMPARISON TO GOES-8

A GOES-8 full disk image comparable to the GOES-9 image was examined for the kind of anomalies noted above. Nothing significant was found.

The following GOES-8 power spectra in Figs. 7-1, 7-2 and 7-3 should be compared to the corresponding GOES-9 Figs. 4-3, 4-4 and 4-5. In each series, the composite power spectra for detector 0 are plotted for sampling ranges 2-16, 8-64 and 32-256, respectively. Overlap in the sampling range is provided for continuity.

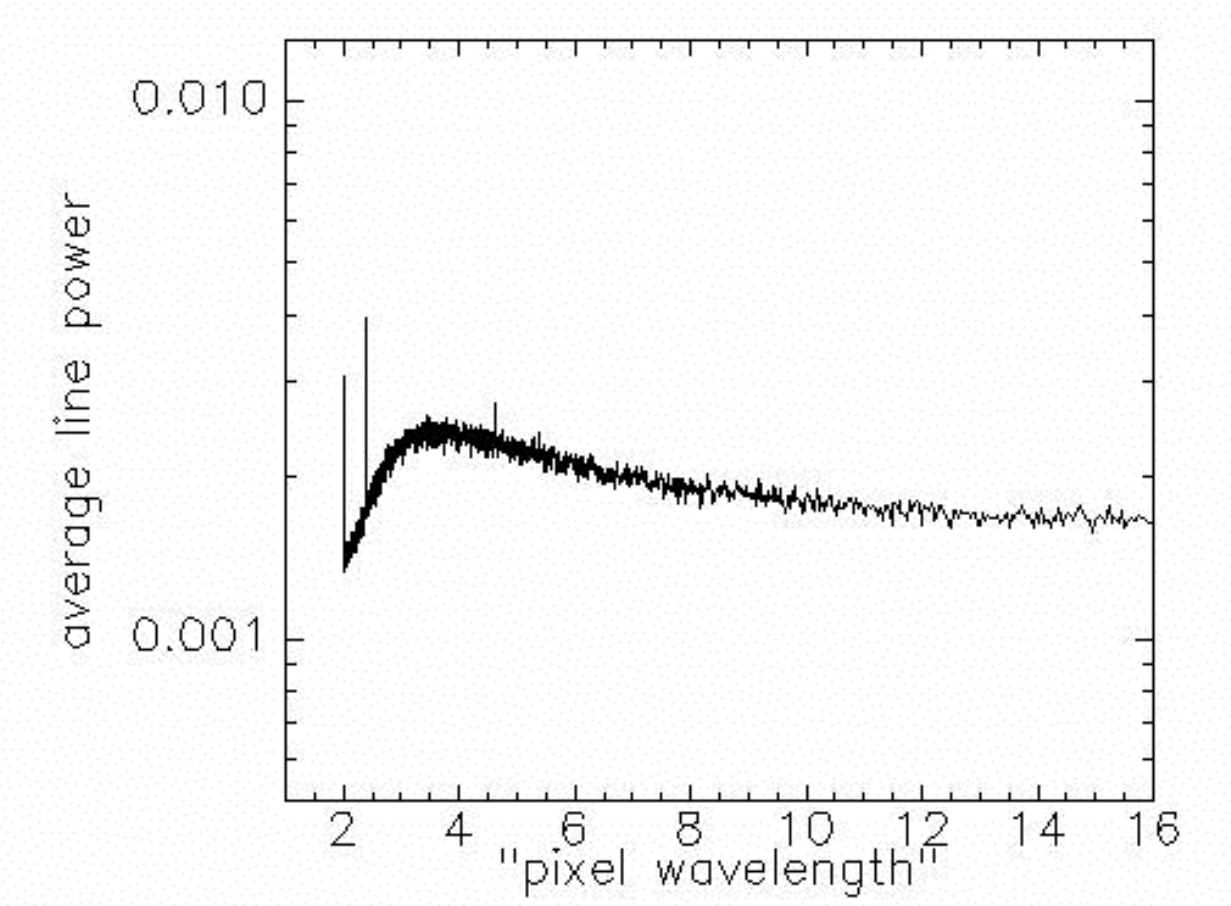

Fig 7-1: Composite power spectral density from the westernmost dark field 4096 samples from all GOES-8 scan lines seen by logical detector 0. Power is plotted on a logarithmic scale versus sampling interval for the sampling range 2-16.

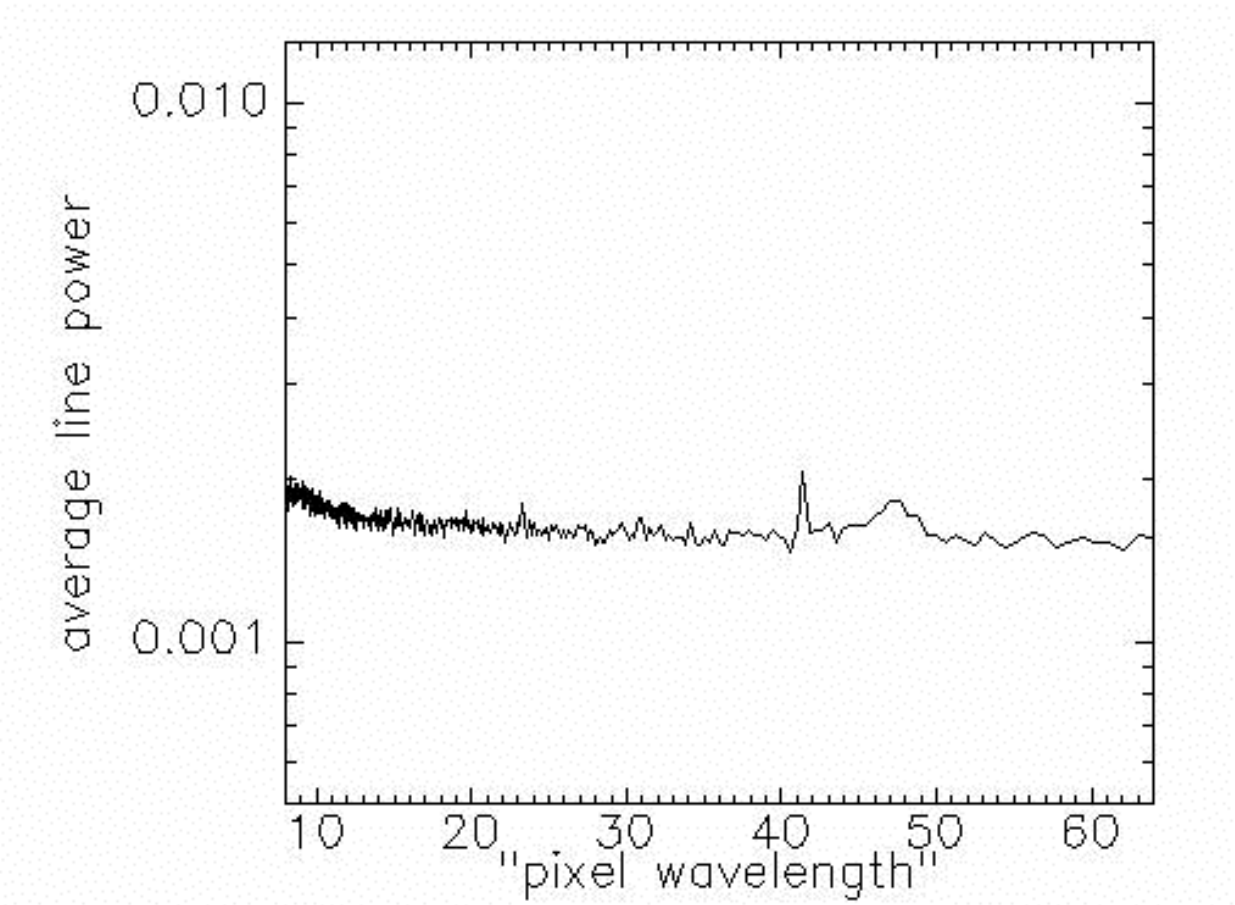

Fig 7-2: Composite power spectral density from the westernmost dark field 4096 samples from all GOES-8 scan lines seen by logical detector 0. Power is plotted on a logarithmic scale versus sampling interval for the sampling range 8-64.

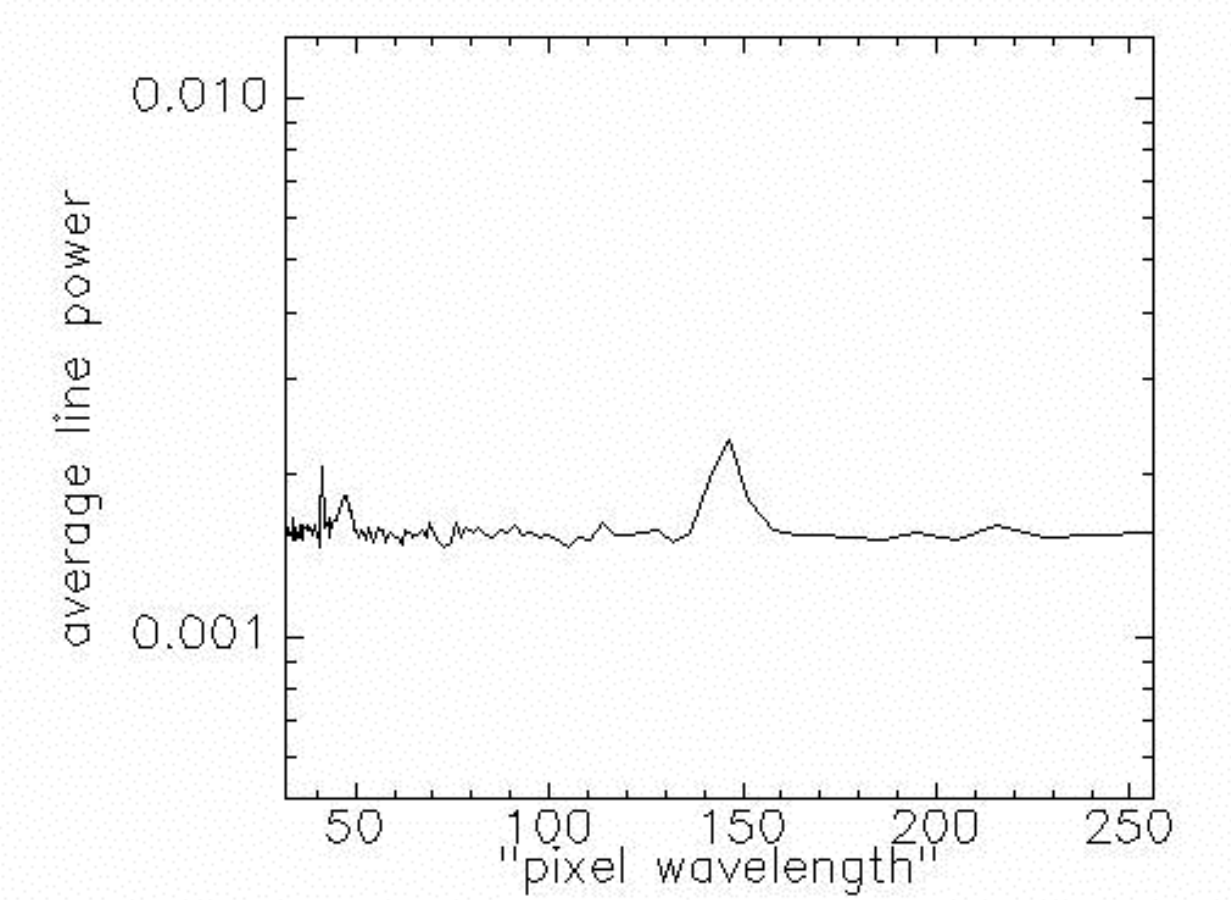

Fig 7-3: Composite power spectral density from the westernmost dark field 4096 samples from all GOES-8 scan lines seen by logical detector 0. Power is plotted on a logarithmic scale versus sampling interval for the sampling range 32-256.

In contrast to the GOES-9 strong resonances at 3, 4 and 5-to-6 sampling rates in Fig 4-2, Fig 7-1 indicates that GOES-8 has a very weak resonance in the 3-to-4 sample rate. Fig. 7-2 indicates no detectable GOES-8 resonances in the 8 to 64 sample range. Finally, Fig. 7-2 indicates a weak resonance at 150 samples that is very similar to the GOES-9 resonance shown in Fig. 4-5. The underlying electrical-mechanical driver for the weak 150 sample resonance on both GOES-8 and GOES-9 is unknown, if there is one.

HYPERLINKS

This report is available in PDF format on a public web site:
http://rsd.gsfc.nasa.gov/goes/text/goes9noise/goes9noise.pdf

The far more detailed supporting analyses are available on the public web site
http://rsd.gsfc.nasa.gov/goes/text/goes9noise/index.html